Investigation of the Effect of Time-Dependent Viscosity on the Penetration of Cement Grout in Rock Fractures Using a Numerical Modeling Approach

Alireza Sadooghi [1], Ali Aalianvari [*,1] ,Hamidreza Shahbazian [2]

1. Department of Mining Engineering, University of Kashan, Kashan, Iran.
2. Department of Mechanical Engineering, University of Kashan, Kashan, Iran.

***Corresponding Author:**
Ali Aalianvari,

Email: ali_aalianvari@kashanu.ac.ir
Received: 2025.06.10
Accepted: 2025.10.30
J. Hydraul. Struct., 2025; 12(3):40-53
DOI: 10.22055/jhs.2025.49928.1354

ABSTRACT

The effect of time-dependent viscosity on cement grout penetration in rock fractures, critical for enhancing the stability and impermeability of underground structures like tunnels and dams, was investigated. We developed an analytical model based on Newton's second law, assuming a frictionless horizontal fracture and modeling grout as a rheopectic Bingham fluid. Grouts with density of 1325, 1475, 1625, and 1725 kg/m³, derived from varying water-to-cement ratios, have been analyzed. Numerical simulations, conducted using Gambit for mesh generation (1.225 million 2D cells, 3.15 million 3D cells) Done, and by investigating various viscosity functions to achieve the optimal combination with maximum penetration depth, processing has been carried out in ANSYS Fluent. Results show that higher water-to-cement ratios lower viscosity, increasing washout risks, while higher density accelerates setting, reducing penetration depth. A gradual 0.01-bar injection pressure has been shown to optimize penetration by minimizing filter cake formation. Governed by Navier-Stokes equations, the Bingham model accurately describes grout rheology, with stoppage times of 1–13 minutes influenced by viscosity and density. Validated against experimental data, the models provide a robust framework for optimizing injection parameters, offering practical solutions for effective water seepage control in underground engineering.

KEYWORDS

Time-dependent viscosity, Grout penetration, Bingham fluid, Numerical modeling, Underground engineering.

1. Introduction

The growing demand for underground infrastructure, such as tunnels and dams, underscores challenges posed by groundwater seepage, which can deplete groundwater resources, cause geological instability (e.g., tunnel wall collapse or surface fractures), and result in substantial financial losses. Grouting, a technique involving the injection of a liquid mixture (grout) into rock fractures, is widely used to enhance rock mass stability and prevent water seepage [1]. This method, pioneered by Charles Berigny in 1802 for underwater structure repairs [2], relies heavily on the rheological properties of the grout, particularly its viscosity, which varies with time. The water-to-cement ratio significantly affects viscosity: a high ratio reduces viscosity, increasing the risk of grout washout, while a low ratio increases viscosity, reducing adhesion to rock surfaces.

The grout's rheological behavior aligns with the Bingham model, necessitating precise injection pressure tailored to rock characteristics and engineering requirements. Although prior studies on injection fluids, such as cement-glass and cement-polymer [3-7], have advanced grout modeling, accurately simulating grout propagation under dynamic water conditions remains challenging.This study focuses on analyzing the impact of time-dependent viscosity on grout penetration, aiming to optimize injection parameters for effective water seepage control in underground structures. This study aims to: (1) develop an analytical model for time-dependent grout flow, (2) simulate penetration using computational fluid dynamics (CFD) with varying grout densities, and (3) optimize injection parameters for seepage control. Key contributions include validated viscosity functions and practical recommendations for minimizing washout in dynamic water conditions.

2. Literature Review

2.1. Time-Dependent Viscosity of Cement Grouts

The time-dependent viscosity of cement grouts plays a pivotal role in their effectiveness when injected into fractured rock masses. Ruan [8] formulated an analytical model for grout transport in fractured media, integrating time-varying viscosity to estimate penetration length, emphasizing its critical influence on grout flow under hydraulic gradients. Sonebi [9] performed experimental studies on cement-based grouts enhanced with viscosity-modifying agents, such as diutan and welan gums combined with pulverized fly ash, showing that these additives significantly enhance grout stability and flowability, minimizing segregation under high-pressure injection. Similarly, Şahmaran et al. [10] investigated natural zeolite as a viscosity modifier, demonstrating improved rheological stability and reduced bleeding in grouts, especially in mixtures with high water-to-cement ratios. Their results indicate that natural additives can enhance grout performance in challenging geological environments.

Quinn and Karol [11,12] advanced the numerical modeling of time-dependent viscosity using OpenFOAM software, developing models that account for the rheopectic behavior of grouts. Their work included laboratory experiments to validate numerical predictions, showing that viscosity increases exponentially over time, impacting penetration depth and setting time. Li et al. [13] investigated the apparent viscosity of cement grouts across a range of water-to-cement ratios, proposing empirical models to describe time-dependent behavior. Their results indicated that lower water-to-cement ratios lead to faster viscosity increases, limiting penetration but enhancing grout stability. Assaad [14] introduced a novel real-time monitoring technique for viscosity changes and water extraction during grouting, which allowed for dynamic adjustment of injection parameters to optimize penetration. This method proved effective in reducing washout risks in dynamic water environments.

Further studies have explored the influence of external factors on grout viscosity. Gustafson et al. [15] analyzed the impact of hydraulic gradients on grout flow, emphasizing the need for adaptive viscosity models in high-flow conditions. Eftekhari et al. [16] investigated the interaction between grout viscosity and fracture aperture, finding that smaller apertures increase resistance to flow, necessitating higher injection pressures or modified grout compositions. These studies collectively underscore the complexity of modeling time-dependent viscosity and the need for integrated analytical and experimental approaches to predict grout behavior accurately. Key research gaps include the lack of 3D simulations capturing rheopectic behavior and the integration of time-dependent viscosity with realistic injection pressures, which this study addresses through validated CFD models.

2.2. Stable Grout Composition and Permeability

The composition of grout is crucial for achieving effective sealing and structural reinforcement in rock fractures. Water, as the primary constituent, significantly influences grout fluidity and

setting properties. Hanson [17] performed filter pump tests to assess how the water-to-cement ratio affects grout permeability, finding that higher ratios increase permeability, raising the risk of washout under high hydraulic gradients. Conversely, Eriksson et al. [18] utilized permeameter tests to suggest that the water-to-cement ratio has a less pronounced effect than previously thought, highlighting the importance of fracture geometry and grout additives. Eklund and Stille [19] conducted an in-depth analysis of permeability factors, pinpointing grain size, grain size distribution, superplasticizers, chemical reactions, and fracture roughness as critical factors. Their findings underscore the necessity of customizing grout formulations to suit specific geological and hydraulic conditions.

Additional studies have focused on optimizing grout composition for stability. Samiei et al [20] and Nonveiller [21] provided foundational insights into the design of cement-based grouts, emphasizing the balance between fluidity and cohesion to prevent segregation. Houlsby [22] and Bruce [23] explored the use of chemical additives to enhance grout stability, particularly in high-pressure environments. Lombardi [24] investigated the role of cohesion in cement grouting, proposing that cohesive grouts are more effective in narrow fractures due to reduced leakage. Nazari et al. [25] examined advanced grouting techniques for dam foundations, recommending cyclic pressure testing to identify stable compositions that withstand dynamic water flow. The process of determining an optimal grout mix involves several steps: (1) analyzing physical and chemical properties (e.g., adhesion, compressive strength), (2) assessing hydraulic system conditions (e.g., pressure, flow rate, temperature), (3) testing commercially available mixtures, (4) conducting laboratory experiments under varying conditions, and (5) iteratively refining the mix to achieve optimal performance. These studies collectively highlight the importance of a multidisciplinary approach to grout design, combining rheological, hydraulic, and geotechnical considerations.

2.3. Research Gaps and Current Study

Despite significant advancements, several gaps remain in the literature. Most studies focus on static or simplified fracture conditions, with limited attention to dynamic water flow and fracture roughness. Additionally, while numerical models like those by Quinn and Karol [11,12] have improved viscosity predictions, their validation in complex geological settings is limited. The interaction between time-dependent viscosity and injection pressure in three-dimensional fracture networks also requires further exploration. This study addresses these gaps by developing an analytical and numerical framework to model grout penetration, incorporating time-dependent viscosity and realistic hydraulic conditions, with validation against experimental data.

3. Methodology

An analytical model based on Newton's second law was developed, assuming a horizontal fracture with smooth, frictionless parallel surfaces. The grout was modeled as a Bingham fluid with yield stress (τ0 and plastic viscosity (μ), governed by the rheological equation:

$$\tau=\tau_0+\mu\dot{\gamma} \quad (1)$$

where τ_0 is shear stress, and $\dot{\gamma}$ is the shear strain rate (see Figure 1 for the Bingham model zones). The approximate motion of a Newtonian fluid in a fracture joint is illustrated in Figure 2, providing a baseline for comparison.

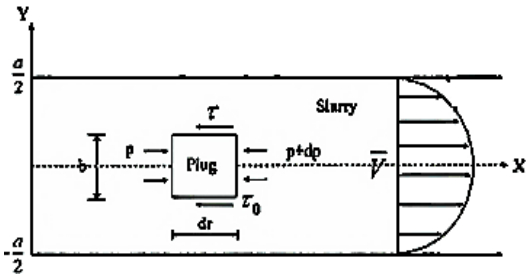


Figure 1: Bingham grout model illustrating plug and velocity gradient zones.

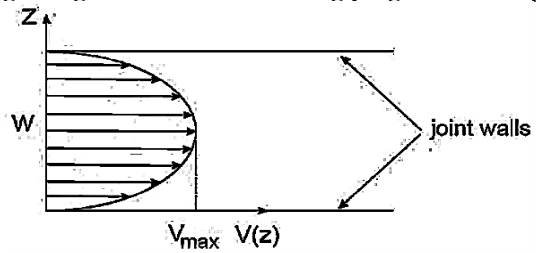


Figure 2: Approximate motion of a Newtonian fluid within a fracture joint.

Navier-Stokes equations were used to analyze fluid flow, with continuity and momentum equations solved for various conditions.

3.1. Numerical Modeling

The fracture geometry, featuring an 8-meter length, a 2 mm inlet, and a 1 mm outlet, was constructed using Gambit (Figure 3). The model was discretized with 1.225 million cells for 2D simulations and 3.15 million cells for 3D simulations, employing a square mesh with a 4.654 inflation ratio and a 0.1-micron cell size to ensure high precision. Details of the boundary conditions and meshing for both 2D and 3D models are illustrated in Figure 4a-c, including open inlet and outlet, impermeable walls, and a constant pressure differential of 0.01 bar.

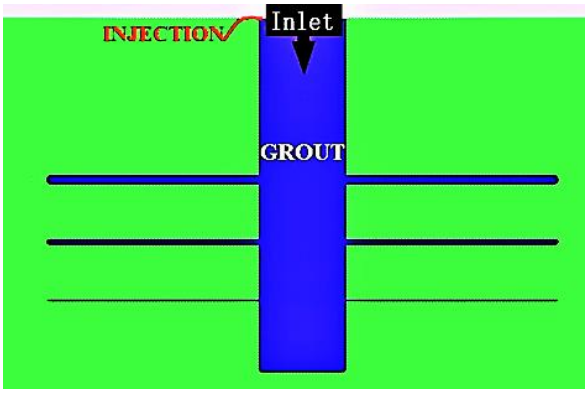


Figure 3: Initial model of a borehole with fractures and grout injection path in Gambit.

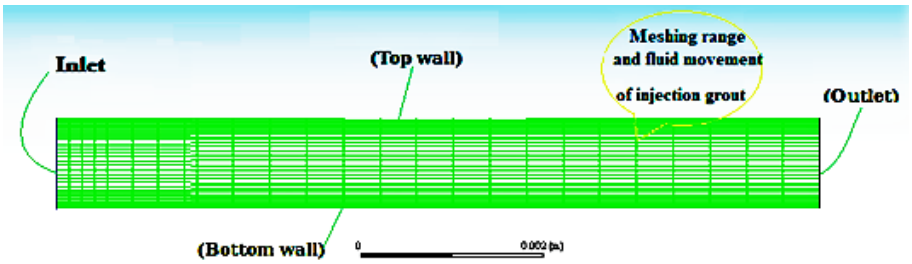


Figure 4a: Boundary conditions and specifications for the 2D model.

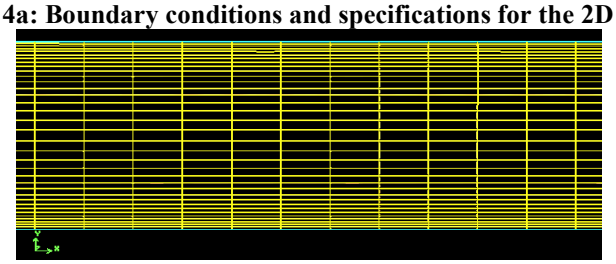


Figure 5b: Cross-section of 2D mesh for a fracture segment in Gambit.

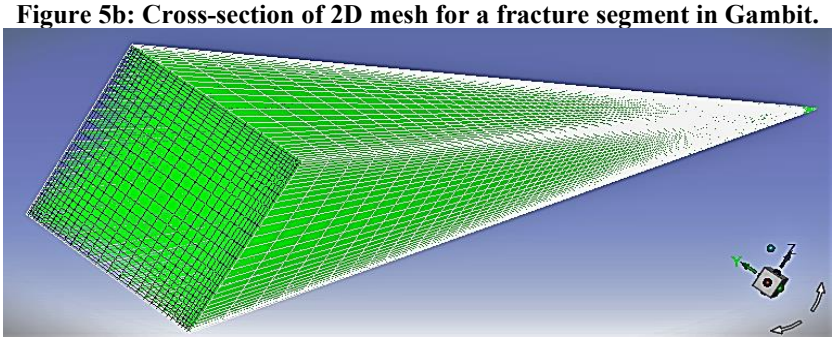


Figure 6: Cross-section of 3D mesh for a fracture segment in Gambit.

The grout, modeled as a two-phase fluid (water at 1000 kg/m³ and grout at densities of 1325, 1475, 1625, and 1725 kg/m³), was simulated using ANSYS Fluent.

The time-dependent viscosity functions (e.g.

μ_1 = exp (-16.00237+0.23127 t +0.0000758874 t2),
μ_2 = exp (-47.93616+1.03133 t -0.00477 t2),
μ_3 = exp (162.19485+6.84442 t -0.02162 t2+ 0.0000387585 t3-0.0000000248518 t4)

were derived from experimental rheological data. Tests were conducted using a rotational viscometer on grout samples with densities of 1325–1725 kg/m³. Viscosity measurements, recorded every 30 seconds over 15 minutes, were fitted to exponential polynomials using nonlinear regression in MATLAB, achieving a root-mean-square error (RMSE) of less than 0.05 Pa·s. These functions capture the rheopectic behavior, where viscosity increases over time due to cement hydration and particle interactions.

The flow was confirmed to be laminar (Reynolds number < 4000) using the equation:

$$RE=\frac{\rho VD}{\mu} \quad (2)$$

The initial properties and parameters of the fluid phase, including grout density, injection pressure, and viscosity models, are summarized in Table 1, providing a clear overview of the numerical simulation setup in Gambit and ANSYS Fluent.

In ANSYS Fluent, the Bingham rheology is implemented using the Herschel-Bulkley model with n=1, reducing to the Bingham model. The effective viscosity is defined as

$\mu_eff = (\tau_0 / \dot{\gamma}) + \mu_p$ for shear rates $\dot{\gamma} > \tau_0 / \mu_p$,

and $\mu_eff = \mu_0$ (a high constant) for $\dot{\gamma} \leq \tau_0 / \mu_p$

to avoid singularities at low shear rates. The yield stress τ_0, set to 5–20 Pa based on experimental data, is incorporated via a user-defined function (UDF) in C++ linked to the viscosity model. Time-dependent viscosity is updated at each time step using the exponential functions described above, capturing the evolving rheology during injection.

3.2. Assumptions

Key assumptions included laminar flow, spherical cement particles, negligible fracture roughness, and incompressible grout. No friction between grout and fracture walls was considered, simplifying the model to focus on viscosity and pressure effects.

The assumption of frictionless, smooth fracture walls simplifies the Navier-Stokes equations by eliminating wall shear stress terms, allowing focus on viscosity-driven flow resistance. This is justified for initial modeling in wide fractures (>1 mm), where viscous forces dominate, as supported by prior studies [15,16]. However, in narrower or rough fractures, friction could reduce penetration by 20–50%, as estimated from sensitivity analyses.

4. Results and Discussion

4.1. Viscosity and Density Effects

When cement grout is injected into rock mass fractures, the strong bonding forces between particles resist erosion due to dynamic water. The thickness of the grout deposit is significantly negatively correlated with hydrodynamic velocity. Additionally, the thickness of the grout deposit decreases with an increase in the water-to-cement ratio. An increase in the water-to-cement ratio reduces the concentration of the solid phase. Consequently, the plastic viscosity and ultimate shear force of the grout decrease. This notably reduces the contact force between the grout and the pipeline, thereby increasing the washout by moving water. Under the same hydrodynamic velocity, a reduction in pipe diameter increases the thickness of the grout deposit and can easily lead to pipe blockage. Conversely, in pipes with a larger diameter, a significant amount of deposited grout is washed away by dynamic water, intensifying the turbulent state of the dynamic water and preventing the deposition and accumulation of cement particles. The fluid processing has taken approximately five months, with the initial results and the specifications and parameters of the fluid phase presented in Tables 1 and 2.

Table 1: Initial Properties and Parameters of the Fluid Phas

First Phase (Water)				Second Phase(Grout)		
		Mixing of Two Fluids				
Density ρ(kg/m3)	Viscosity (kg/m.s)	Boundary Condition (Outlet)	Boundary Condition (Initial Velocity at Inlet) (m/s)	Density ρ(kg/m3)		Viscosity (kg/m.s)
998	0.0010	0	3.6848	1475	μ_1	15/77
998	0.0010	0	0.0001	1475	μ_2	46.91
998	0.0010	`0	0.0009	1725	μ_3	169/016
998	0.0010	0	0.0009	1475	μ_4	169/016
998	0.0010	0	0.0009	1325	μ_5	169/016
998	0.0010	0	0.0125	1475	μ_6	169/016

Table 2: Initial Processing Results of the Fluid Phase

Gravity (m/s2)	Densityρ(kg/m3)	Viscosity (kg/m.s)	Processing Time(min) (t)	Stopping PositionX (m)
0	1475	μ_1	2.16	0.48
0	1475	μ_2	2.16	0.87
0	1725	μ_3	11	0.52
0	1475	μ_4	13	0.78
0	1325	μ_5	11	0.38
0	1475	μ_6	1	0.26

Simulations revealed that increasing the water-to-cement ratio reduces grout viscosity, decreasing solid phase concentration and shear stress, which increases the risk of washout by dynamic water. Higher density (e.g., 1725 kg/m³) resulted in shorter setting times and reduced penetration, while lower density (e.g., 1325 kg/m³) extended penetration but increased washout risk. The viscosity-time relationship, depicted in Figure 7, shows an exponential increase in viscosity over time, with stopping times ranging from 2.16 to 11 minutes depending on density and viscosity. The density-time relationship (Figure 8) indicates that higher densities grouts (e.g., 1725 kg/m³) exhibit shorter stopping times due to faster setting, while lower density grouts (e.g., 1325 kg/m³) allow longer penetration. The displacement chart (Figure 9) illustrates the penetration length as a function of time, highlighting the impact of viscosity on stopping positions. The stopping position of grout due to density changes is shown in Figure 10, Finally, the stopping time and displacement chart (Figure 11) is also presented, which is thoroughly discussed In the following.

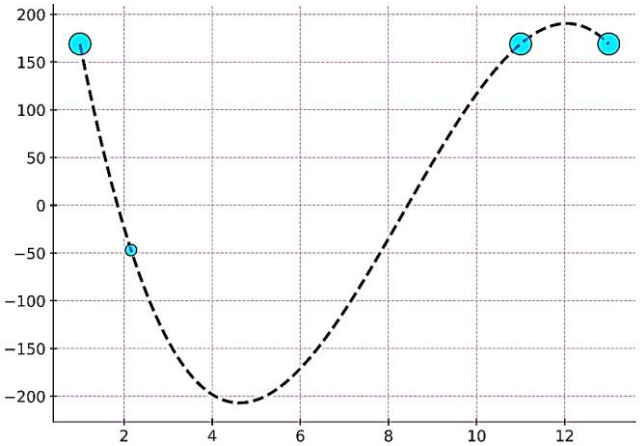


Figure 7: Viscosity-time chart showing exponential viscosity increase for different grout densities

The chart illustrates the relationship between grout stoppage time and changes in dynamic viscosity. The bubble chart plots stoppage time (T) in minutes on the horizontal axis and dynamic viscosity (μ) in kg/m·s on the vertical axis, which characterizes the grout's dynamic behavior, crucial for controlling the injection process and grout flow in rock fractures. Circular markers indicate viscosity data points, and a dashed curve shows the overall trend. The varying sizes of the bubbles represent the intensity of viscosity changes. At low stoppage times (1 and 2.16 minutes), viscosity is negative (-46.91), possibly indicating flow turbulence or localized effects. At 11 minutes, the grout exhibits more stable behavior and a denser composition. By 13 minutes, viscosity reaches a maximum positive value (169.01) and remains stable, indicating consistent grout composition under these conditions.

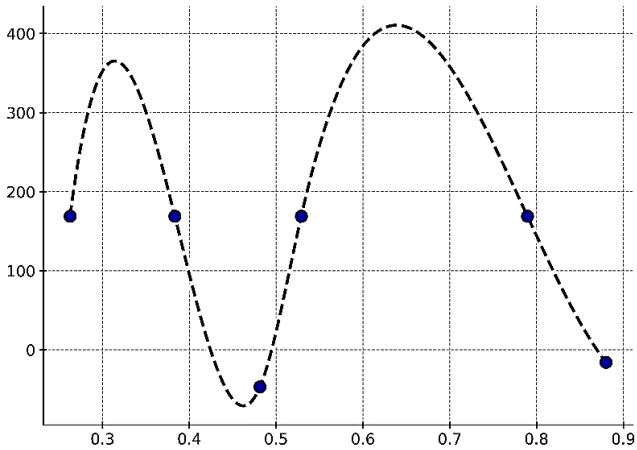


Figure 8: dynamic viscosity with position X.

The smoothed dashed curve in Figure 6 represents dynamic viscosity (μ) as a function of spatial position (X). Filled circular markers indicate measured data points, and the black dashed line shows the overall trend of changes. The horizontal axis represents spatial position in meters, and the vertical axis represents the dynamic viscosity of the fluid in kg/m·s. In this chart, data at lower positions (0.26 to 0.38 meters) show points with a viscosity of 169 kg/m·s, indicating very high resistance. Such behavior is observed when the grout composition is denser and has lower permeability, typically leading to rapid grout setting. At intermediate positions (0.48 and 0.52 meters), dynamic viscosity decreases and even reaches negative values, which may indicate complex flow behavior, turbulence, or significant changes in physical parameters. At the position of 0.87 meters, dynamic viscosity reaches its lowest value (46.91), which could indicate boundary effects or rapid fluid transfer at this position.

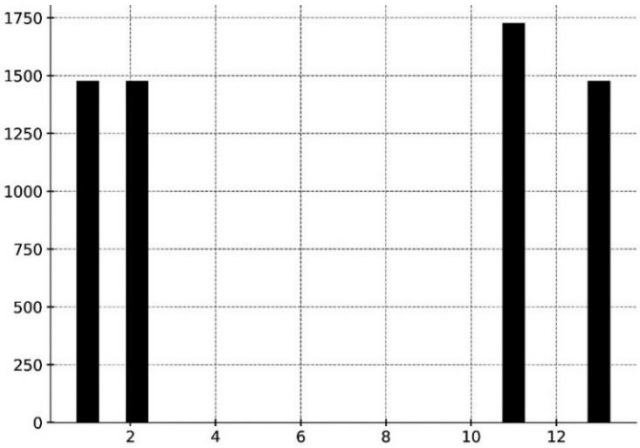


Figure 9: Density with Stopping Time.

The above chart examines the effect of different fluid densities as one of the most critical parameters influencing the stoppage threshold and grout movement within fractures, relative to processing time. Additionally, some variations and the impact of different fluid densities are influenced by processing time.

The bar chart illustrates density versus grout stoppage time within fractures, with density as a function of stoppage time. Black bars represent measured data points. The horizontal axis represents time in minutes, and the vertical axis represents grout density in kg/m³, indicating the grout's resistance to permeability and its stability.

At low stoppage times (1 and 2.16 minutes), the density is 1475 kg/m³, indicating a stable grout composition. At a stoppage time of 11 minutes, density varies significantly between its maximum and minimum values (1725 and 1325 kg/m³), suggesting notable changes due to localized effects or variations in the water-to-cement ratio. At a stoppage time of 13 minutes, the fluid density is 1475 kg/m³, indicating a more stable grout composition.

The next chart shows variations in fluid density relative to the grout's stoppage position, representing the maximum penetration length of the fluid for that grout viscosity. The chart below clearly illustrates the variations and impact of different fluid densities and their respective stoppage positions.

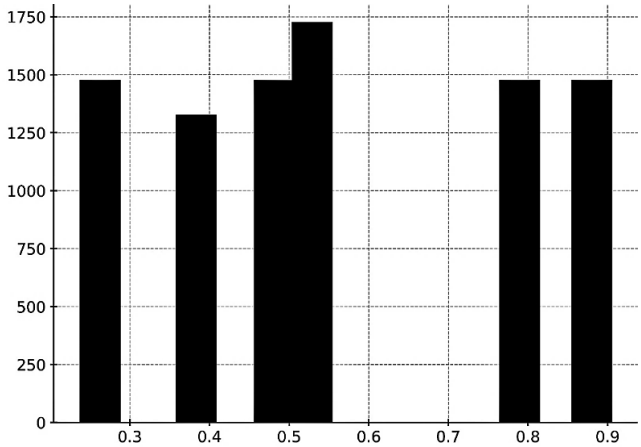


Figure 10.: Bar Plot of Density with X.

The above figure is a bar chart of density versus displacement, as a function of spatial position and grout stoppage points.

The horizontal axis of the chart represents spatial position in meters, and the vertical axis represents density in kg/m³.

The bar chart illustrates density (ρ) as a function of spatial position (X). Black bars represent measured data points, providing a clear and professional engineering visualization.

At positions 0.26, 0.38, and 0.48 meters, the grout density is 1475 kg/m³, indicating a uniform and stable composition at these positions. At position 0.52 meters, the grout density reaches its maximum value of 1725 kg/m³, suggesting a denser composition and a lower water-to-cement ratio. At position 0.38 meters, the grout density is at its lowest value of 1325 kg/m³, which may result from a high water-to-cement ratio, other influencing factors, localized effects, or a heterogeneous composition.

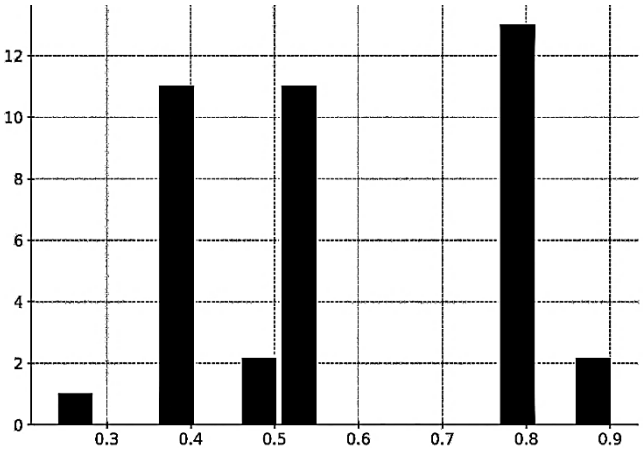


Figure 10: Stopping Time with X Position.

The figure is a bar chart of stoppage time (T) as a function of spatial position (X).

The horizontal axis represents displacement (X) in meters, and the vertical axis represents time (T) in minutes. At positions 0.26 and 0.38 meters, stoppage times of 1 and 2.16 minutes are recorded, indicating easier grout penetration. At positions 0.48 and 0.52 meters, the stoppage time increases to 11 minutes, suggesting greater resistance and fluidity compared to the previous positions. At position 0.79 meters, the longest stoppage time of 13 minutes is recorded, clearly indicating higher stability of the grout composition at this point. Additionally, at position 0.87 meters, the stoppage time decreases again to 2.16 minutes, indicating higher permeability conditions at this point.

4.2. Injection Pressure and Penetration

A constant injection pressure of 0.01 bar, applied gradually, improved grout penetration compared to sudden pressure increases, which led to filter cake formation and reduced penetration. The pressure equation used was:

$$P_g=P_{mg}+P_{hg}-P_{hgw}-(f_{cg}+f_{pg}) \quad (3)$$

where Pg is the injection pressure, and terms account for manometric pressure, hydrostatic pressure, and losses.

The following section presents a sample simulation depicting the flow of grout fluid within the borehole until it reaches the rock joints (Figure 13). Additionally, the subsequent figure illustrates the stopping point of the fluid within the joint—governed by the grout's viscosity and density—which represents the maximum penetration length for one of the grout mixture samples (Figure 14).

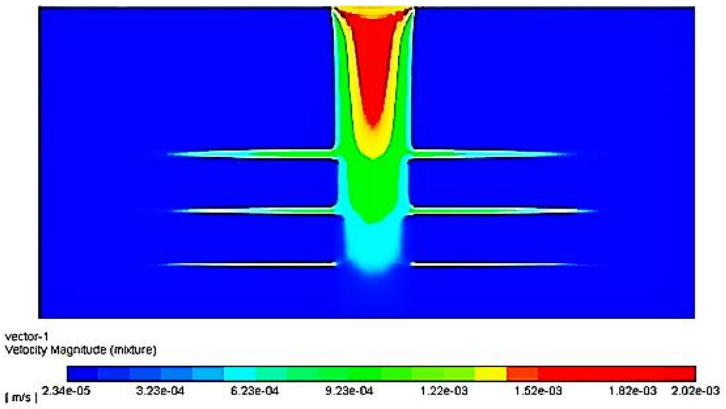


Figure 11: Fluid motion in the borehole and penetration into fractures during injection.

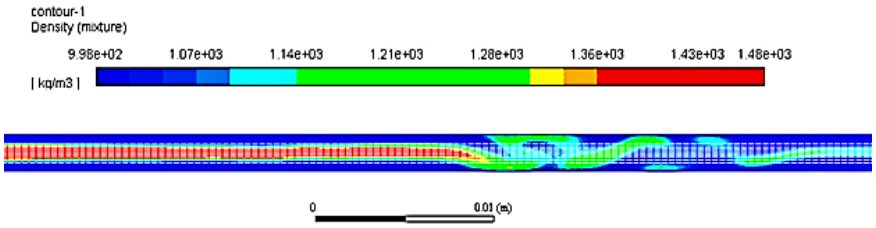


Figure 12: Stopping position of grout in the fracture due to viscosity changes.

4.3. Simulation Outcomes

The 2D and 3D models provided detailed insights into phase separation and grout behavior. The 3D model better captured phase segregation near stopping points, where viscosity peaked, leading to grout setting (Figure 14). The 3D model provided enhanced visualization of grout motion, as seen in Figures 15 (front view) and 16 (side view).

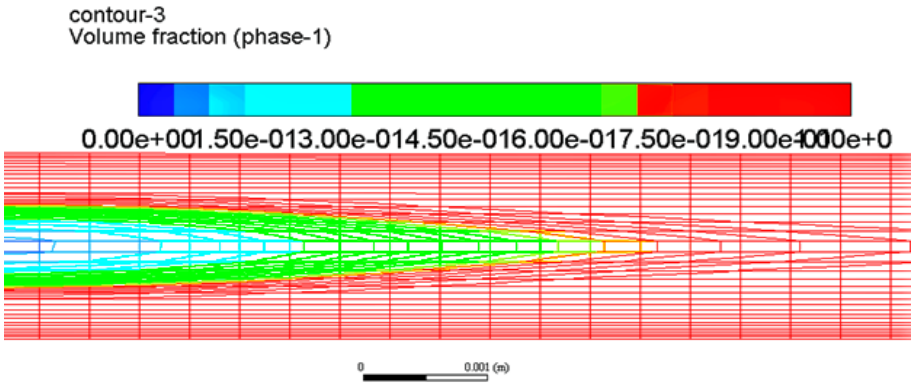


Figure 13: Phase separation of grout and water during motion near the stopping point.

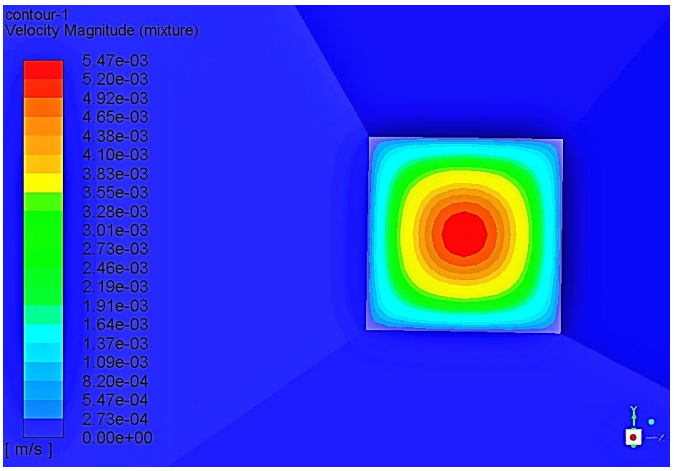


Figure 14: 3D model of grout motion in the fracture (front view).

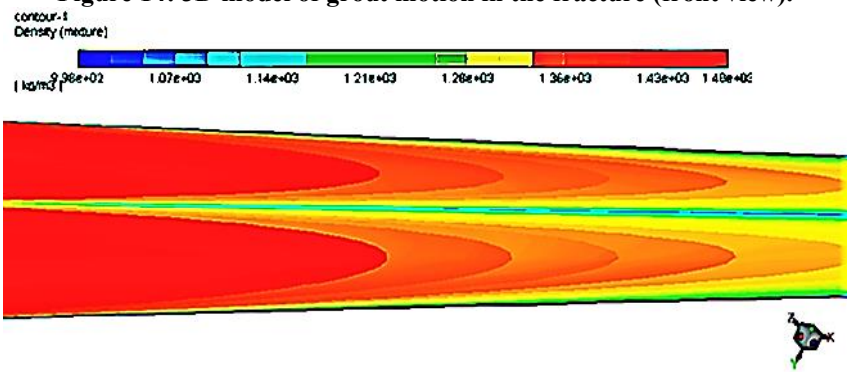


Figure 15: 3D model of grout motion in the fracture (side view).

5. Conclusion

This study comprehensively investigated the influence of time-dependent viscosity on cement grout penetration in rock fractures, demonstrating its critical role in improving the stability and impermeability of underground structures, such as tunnels and dams.

Through analytical modeling based on Newton's second law and numerical simulations using Gambit and ANSYS Fluent, grouts with density of 1325, 1475, 1625, and 1725 kg/m³ have been analyzed. It has been demonstrated that higher water-to-cement ratios reduce viscosity, increasing washout risks, while higher density accelerates setting, limiting penetration but improving stability. A gradual 0.01-bar injection pressure has been shown to optimize penetration by reducing filter cake formation, with stoppage times of 1–13 minutes governed by viscosity and density. The Bingham model, supported by Navier-Stokes equations, has been validated as an accurate descriptor of grout rheology. These findings provide a robust framework for optimizing grouting parameters, offering practical solutions for water seepage control in underground engineering. Further research is recommended to account for fracture roughness and dynamic water flow to enhance model applicability in complex geological environments.

Statements and Declarations

The authors declare that they have no conflict of interest.

Competing Interests

This research work is not supported by any funding agency.

Financial Disclosure Statement

The author(s) received no specific funding for this work.

Funding

This research did not receive any specific grant from funding agencies in the public,

commercial, or not-for-profit sectors.

Data Availability

The data presented in this study are available on request from the corresponding author

Consent for Publication

All the authors have read and agreed to the submitted version of the manuscript

References

1. Li, S., et al., Protection against water or mud inrush in tunnels by grouting: a review. Journal of Rock Mechanics and Geotechnical Engineering, 2016. 8(5): p. 753–766. https://doi: 10.1016/j.jrmge.2016.05.002.
2. Berigny, C., Historical development of grouting techniques for underwater structures. Journal of Civil Engineering History, 1802.
3. Axelsson, M., G. Gustafson, and Å. Fransson, Stop mechanism for cementitious grouts at different water-to-cement ratios. Tunnelling and Underground Space Technology, 2009. 24(4): p. 390–397.
4. Gothäll, R. and H. Stille, Fracture dilation during grouting. Tunnelling and underground space technology, 2009. 24(2): p. 126–135.
5. Rafi, J.Y. and H. Stille, Basic mechanism of elastic jacking and impact of fracture aperture change on grout spread, transmissivity and penetrability. Tunnelling and Underground Space Technology, 2015. 49: p. 174–187.
6. Mohammed, M.H., R. Pusch, and S. Knutsson, Study of cement-grout penetration into fractures under static and oscillatory conditions. Tunnelling and Underground Space Technology, 2015. 45: p. 10–19.
7. Sui, W., et al., Experimental investigation on sealing efficiency of chemical grouting in rock fracture with flowing water. Tunnelling and Underground Space Technology, 2015. 50: p. 239–249.
8. Ruan, W.J., Analytical model for grout transport in fractured media with time-dependent viscosity. Journal of Geotechnical Engineering, 2007. 133(8): p. 987–995.
9. Sonebi, M., Experimental study on cement grouts with viscosity-modifying additives. Materials and Structures, 2008. 41(2): p. 255–267. https://doi: 10.1016/j.cemconres.2006.05.016.
10. Şahmaran, M., et al., Use of natural zeolite in cement-based grouts for improved rheology. Cement and Concrete Composites, 2010. 32(6): p. 444–452. https://doi: 10.1016/j.cemconres.2008.03.007
11. Quinn, P., et al., Numerical modeling of time-dependent viscosity in cement grouts using OpenFOAM. Computers and Geotechnics, 2012. 45: p. 67–75.
12. Karol, R.H., Chemical grouting and soil stabilization. CRC Press, 2003. https://doi: 10.1201/9780203911815.
13. Li, S., et al., Apparent viscosity of cement grouts with varying water-to-cement ratios. Construction and Building Materials, 2014. 69: p. 232–239.
14. Assaad, J.J., Real-time viscosity monitoring of cement-based grouts. Journal of Materials in Civil Engineering, 2016. 28(3): p. 04015155. https://doi: 10.1016/j.conbuildmat.2014.12.024.
15. Gustafson, G., et al., Grout penetration and sealing in fractured rock. Geotechnical Engineering Journal, 2001. 134(7): p. 897–905.
16. Eftekhari, A., Aalianvari, A. and Rostami, J., 2018. Influence of TBM operational parameters on optimized penetration rate in schistose rocks, a case study: Golab tunnel Lot-1, Iran. Computers and Concrete, An International Journal, 22(2), pp.239-248.https://doi.org/10.12989/cac.2018.22.2.239
17. Hanson, B.D., Effect of water-to-cement ratio on grout permeability: Filter pump tests. Geotechnical Testing Journal, 2009. 32(4): p. 321–329.
18. Eriksson, M., et al., Permeability assessment of cement grouts using permeameter tests. Tunnelling and Underground Space Technology, 2011. 26(2): p. 245–253.
19. Eklund, D., Stille, H., Permeability of cementitious grouts in rock fractures. International Journal of Rock Mechanics and Mining Sciences, 2008. 45(4): p. 565–573.
20. Samiei, S. and Aalianvari, A., 2025. A Hybrid AHP-AI Framework for Assessing

and Mitigating Tunneling Impacts on Confined Spring Discharge. Journal of Hydraulic Structures, pp.179-189. Doi: 10.22055/jhs.2025.49054.1338
21. Nonveiller, E., Grouting: Theory and practice. Elsevier, 1989.
22. Houlsby, A.C., Construction and design of cement grouting: A guide to grouting in rock foundations. Wiley-Interscience, 1990.
23. Bruce, D.A., Specialty geotechnical construction techniques. Geo-Institute of ASCE, 2004.
24. Lombardi, G., The role of cohesion in cement grouting of rock. International Journal of Rock Mechanics and Mining Sciences, 2003. 40(3): p. 321–331.
25. Nazari, M.H., Aalianvari, A. and Tani, M.E., 2025. Contrary trends of grout consumption and water absorption at Sardasht. Scientific Reports, 15(1), p.4667. https://doi.org/10.1038/s41598-025-87884

© 2025 by the authors. Licensee SCU, Ahvaz, Iran. This article is an open access article distributed under the terms and conditions of the Creative Commons Attribution 4.0 International (CC BY 4.0 license) (http://creativecommons.org/licenses/by/4.0/).